6.0–10.0-MeV/u He^{2+}-ion-induced electron emission from water vapor

D. Ohsawa,[1,*] Y. Sato,[2] Y. Okada,[3] V. P. Shevelko,[4] and F. Soga[2]
[1]*Radioisotope Research Center, Kyoto University, 606-8501 Kyoto, Japan*
[2]*National Institute of Radiological Sciences, Anagawa, 263-8555 Chiba, Japan*
[3]*Tokyo Science University, Yamazaki, 2641 Chiba-Noda, Japan*
[4]*P.N. Lebedev Physical Institute, 119991 Moscow, Russia*
(Received 31 May 2005; published 21 December 2005)

We discuss absolute doubly differential cross sections (DDCS's) for the energy and angular distributions (20°–160°) of secondary electrons produced in the collisions of 6.0- and 10.0-MeV/u He^{2+} ions with water vapor. Details of our experiments were reported in our previous paper [D. Ohsawa *et al.*, Nucl. Instrum. Methods Phys. Res. B **227**, 431 (2005)], which mainly considered the total uncertainty (±13%), as well as absolute DDCS data (7–10 000 eV) by 6.0-MeV/u He^{2+} ions. All DDCS data, including the newly obtained data (20–12 000 eV) by 10.0-MeV/u He^{2+} ions, are compared with classical theories after being corrected for relativistic effects. Based on the Rudd model and the Rutherford cross section, the experimental results are discussed by taking account of the momentum spread of the bound electrons. This paper mainly describes the analysis of low-energy electrons and binary encounter peaks at high energies, as well as details of relativistic corrections.

DOI: 10.1103/PhysRevA.72.062710 PACS number(s): 34.80.Bm, 34.80.Kw, 34.50.Dy

I. INTRODUCTION

There has been a very small amount of cross-section data on electron emission from water vapor produced by the impact of charged particles having energies of several MeV/u or more, particularly by heavy ions including α particles [1]. Such data are highly important from the viewpoint of fundamental biophysics in heavy-ion cancer therapy [2,3], as well as testing theoretical models in radiation physics [4–8]. Studying the track structure of heavy ions in water is motivated by fundamental problems in radiation biology with charged particles [9–11]. Recent understandings have shown that the spatial distribution of energy deposition along a heavy-ion track is related to DNA damage and cell killing. However, the relation between DNA damage and cell killing has not yet been clarified. This problem should be essentially connected to the repair process of DNA molecules after ionization and dissociation [12], which has so far been studied as a subject in chemistry and biology. What can we do to approach this basic subject from the viewpoint of physics? One thing is obviously to give the spatial distribution of energy deposition along a track of 2–10-MeV/u heavy ions in water, which corresponds to the particle energy around the Bragg peak; data of electron emission are thus essential. Our previous paper [13] reported on an apparatus for measuring secondary emission (SE) electrons from water vapor and the data of 6.0-MeV/u He^{2+} ion-induced SE electrons; absolute doubly differential cross sections (DDCS's), at angles of 20°–160° in 10° steps and energies of 7–10 000 eV, were experimentally deduced, and the singly differential cross section (SDCS) was also obtained from measured DDCS values by integration with respect to the ejected angle.

The purpose in this work is to discuss the data of SE electrons ejected from water vapor in collisions of 6.0–10.0-MeV/u He^{2+} ions, from the viewpoint of radiation physics. All of these data are compared with classical models, and the observed results and unexpected discrepancies are discussed. An example of a comparison of the data of 6.0-MeV/u He^{2+} ions with the Rutherford cross-section and Rudd model [14] showed some meaningful and significant discrepancies, except for low-energy electrons [13]. Our angular distributions showed a nearly isotropic emission in the energy range of $<\sim 20$ eV and a symmetric distribution around 90° in ~ 30–200 eV. On the contrary, such phenomena were not observed in Toburen's data of 0.2–0.5-MeV/u He^{2+} ions on the same target [1]. Also, our SDCS data showed a 2–3 times greater yield of high-energy (~ 10 keV) electrons than the Rutherford cross section. These phenomena were mainly analyzed by using the Rutherford cross section, after being modified from the center of mass (c.m.) to the laboratory (Lab) frame, of which the derivation is summarized in Appendix A and by taking account of the momentum spread of the bound electrons (Compton profile) [15] and single- and two-center effects [16], as well as the Fermi-shuttle acceleration mechanism [17–22]. The Fermi-shuttle acceleration model was first introduced by Fermi in order to approach the origin of high-energy cosmic rays. Recently, this model has attracted attention again to be applied to ion-atom collisions, in which the ejected electrons repeat head-on collisions between the projectile and target nucleus, resulting in an accumulative acceleration by a step of $2V$ at maximum, where V is the projectile velocity.

Since high-energy electrons ($\lesssim 12$ keV) are included in our data, relativistic corrections are first made regarding both the required deflector voltage in the energy analyzer and the binary encounter (BE) collision process. The corrected values are, second, compared with the relativistic Rutherford cross section and classical theories. In our case, the β value

*Corresponding author. Electronic address: dohsawa@mbox.kudpc.kyoto-u.ac.jp

(ratio of particle velocity to the light speed) of the projectile is 0.11–0.14 and that of the measured electrons exceeds 0.2, suggesting the necessity of relativistic corrections. Details of these corrections are described in Appendix B. From the viewpoint of the same target, our DDCS data are compared with those obtained by 0.2–0.5-MeV/u He^{2+} ions, in which the energy spectrum and angular distributions are discussed.

II. EXPERIMENT

An outline of our apparatus [13] is given below. The method used is one of the well-known cross-beam techniques, in which incident ions interact with a vertically emitted water-vapor molecular beam. Ejected SE electrons are detected by a Chevron-type microchannel plate (MCP) assembly after being analyzed by a 45°-inclined parallel-plate electrostatic spectrometer, which is rotatable from 20° to 160° with respect to the incident-beam direction. Water vapor is vertically emitted into the interaction region from a nozzle of $1\times 15\text{-mm}^2$ aperture and is instantly frozen and trapped as ice on a stainless-steel panel, which is cooled by liquid nitrogen. With this water-vapor generation and collection system, a stable water-vapor jet (10^{-2}–10^{-3} Torr) was obtained without deteriorating the pressure in the scattering chamber: $\sim 4\times 10^{-7}$ Torr with a vapor flow of 40.0 cm^3/min. Some new techniques allowed us to improve the estimated uncertainty (systematic error) to be on the order of ±13%, except for high-energy electrons.

In a recent measurement with 10.0-MeV/u He^{2+} ions, we tried to evaluate the DDCS's at electron energy down to 1 eV. The measured values, however, were considerably fluctuated due to the magnetic field produced by the ON-OFF control in the dc current for a heater surrounding the nozzle for the emission of water vapor, at which the temperature was stabilized to 100 °C.

In addition, we recently found a significant problem. During 2–3 years of measurements, our chamber (made of iron) was magnetized due to the effects by both the heater and opening and closing process of the upper lid of the chamber for maintenance. In the latter process, slight but frequent collisions between the lid and chamber would produce some magnetization, resulting in a considerable increase in the residual magnetic field (by a factor of ~5) at around the collision center. The lower limit in measurable energies with a small uncertainty has thus been unfortunately changed to ~20 eV in recent measurements from ~7 eV in the early measurements. Meanwhile, the higher limit was slightly improved (increased) from 10 to 12–14 keV by careful operation of the deflector electrode against sparks, though it is still lower than the maximum energy (22.0 keV) in collisions of 10-MeV/u projectiles.

The following modifications will be made for the forthcoming experiments: the chamber will be demagnetized and the power supply for heaters changed to an ac type; the metal panel (made of Cu at present) surrounding the interaction region will also be changed to that made of μ metal, in order to suppress the effects of stray magnetic fields.

III. DEDUCTION OF THE DDCS AND ERROR ANALYSES

Suppose that a beam of N_p ions enters a target of water vapor at density n_t and travels over a path length ℓ. As a result, electrons of kinetic energy W are ejected into a solid angle Ω. Our apparatus permits us to observe the number of analyzed electrons having an energy spread ΔW. The DDCS values of electron emission are obtained from the following equation:

$$\frac{d^2\sigma}{dW\,d\Omega}=\frac{N_{eS}/\exp(-\sigma_s n_t r)-N_{eB}}{N_p\varepsilon t\,\Delta\Omega\,\Delta W\,n_t l}\ \text{cm}^2/\text{eV sr molecule}, \tag{1}$$

where N_{eS} and N_{eB} are the number of total (when the water vapor is turned on) and background (when the water vapor is turned off) counts, respectively. The term $\exp(-\sigma_s n_t r)$ is a compensation factor to correct for the effect of scattering or absorption of ejected electrons within the target before being detected. σ_s is the total scattering cross section for ejected electrons with energy W, n_t is the density of water molecules in the target, and r is the effective path length of secondary electrons passing through the target. The product $n_t r$ is evaluated, depending on the angles. The parameter N_p is the number of incident ions, and ℓ is the effective path length of the incident beam through the target; the product $N_p n_t \ell$ is separately evaluated by taking the ion-beam profile into account; t is the product of t_1 and t_2; t_1 is the transmission efficiency of electrons with mean energy W passing through the spectrometer and collimator; and t_2 is that for the meshes. The ratio $\Delta W/W$ is the full width at half maximum (FWHM) of the spectrometer, and ε is the detection efficiency of the MCP, depending on W. The deduction of these experimental parameters is described in detail in our previous paper [13].

In angles, the measurements were carried out at 20°–160° with 10° steps for both 6.0- and 10.0-MeV/u He^{2+} ions, while in energies 7–10 000 eV for 6.0-MeV/u and 20–14 000 eV for 10.0-MeV/u ions. The DDCS values for 10.0-MeV/u He^{2+} ions were deduced by using exactly the same experimental parameters as those used for 6.0-MeV/u He^{2+} ions. The SDCS was obtained from the measured DDCS values by integration with respect to the ejected angle. In the process of numerical integration, the values between two adjoining angles were interpolated from several angles by cubic spline interpolation, and those for 0°–20° and 160°–180° were extrapolated by the polynomial fitting function.

The total systematic error in the obtained DDCS data was dominated by those for $\Delta\Omega t_1 t_2(\pm 10\%)$, $\varepsilon(\pm 5\%)$, and $N_p n_t \ell(\pm 5\%)$ and was estimated to be ±13% for all measured angles and energies. The statistical error in the measured DDCS's was determined by the net counts ($N_{eS}-N_{eB}$), which depend on both the electron energies and the ejected angle. In the case of 6.0 MeV/u, the statistical error is on the order of 1% at energies smaller than 100 eV and reaches several tens % at ~10 keV. Particularly, at both 20° and 160°, the error exceeds 80%, which is due to x rays induced by the direct impact of the beam halo with the detector housing, resulting in a significant increase in the background counts. However, at 40°–140°, the error is smaller than 30%, even at ~10 keV, and the error of SDCS is sufficiently suppressed down to the order of 10%. In the case of 10.0 MeV/u, a careful adjustment of the He^{2+} beam tuning allowed us to

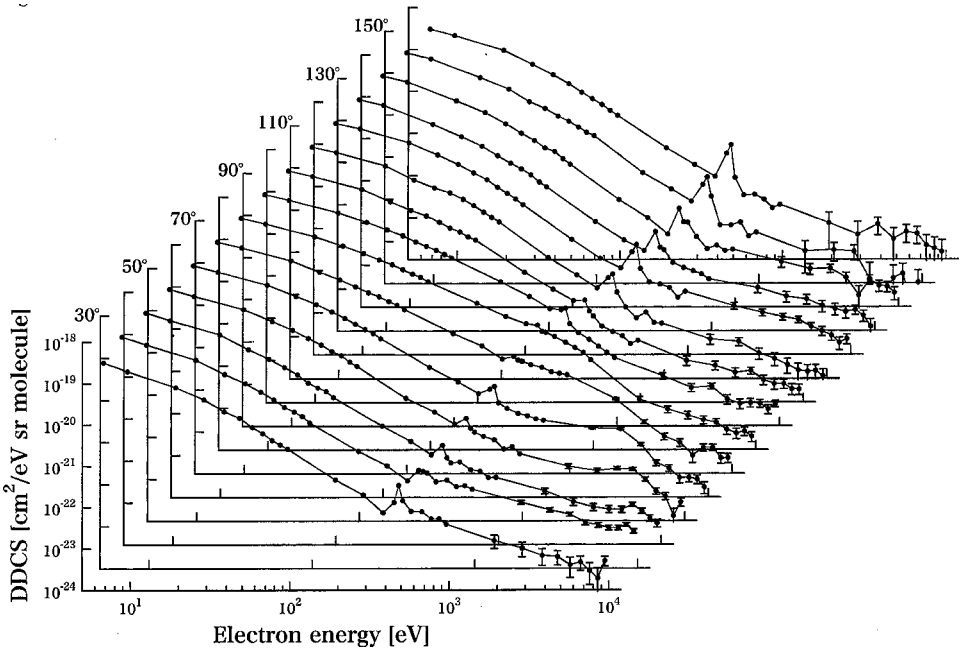

FIG. 1. DDCS's of secondary electrons (7–10 000 eV and 20°–160°) produced in the collision of 6.0-MeV/u He^{2+} ions with H_2O molecules.

reduce the background level by 2/3 at around 60°–120° and 1/3 at both 20° and 160°, compared with the previous measurements with 6.0-MeV/u He^{2+} ions, resulting in a considerable reduction in the statistical error. As a result, the error of SDCS's was reduced to 6%–7%. The total error was evaluated to be 17% and 14% at ~10 keV for 6.0 and 10.0 MeV/u, respectively.

There is a slight angular dependence produced by the geometrical conditions, which is supported by two pieces of evidence: first, the O *KLL* Auger group observed to be isotropic by taking account of masking effects at around 90°; second, the isotropic (±10%) and smooth characteristics observed for low-energy electrons in Figs. 3 and 4, based on the theory of soft collision.

IV. DISCUSSION

A. DDCS

Figures 1 and 2 show the DDCS values of electron emission in collisions of 6.0 and 10.0-MeV/u He^{2+} ions on water vapor, of which the general characteristics are first described in the following.

In both Figs. 1 and 2, one can see that the DDCS values decrease monotonically with an increase of the electron energy, except for clear peaks at ~500 eV and very small peaks at ~1000 eV. These two peaks are attributed to Auger electrons from the 1*s* vacancy in oxygen molecules; the former (~500 eV) should be due to *K-LL* and the latter (~1000 eV) to *KK-LLL* processes, respectively. In a mea-

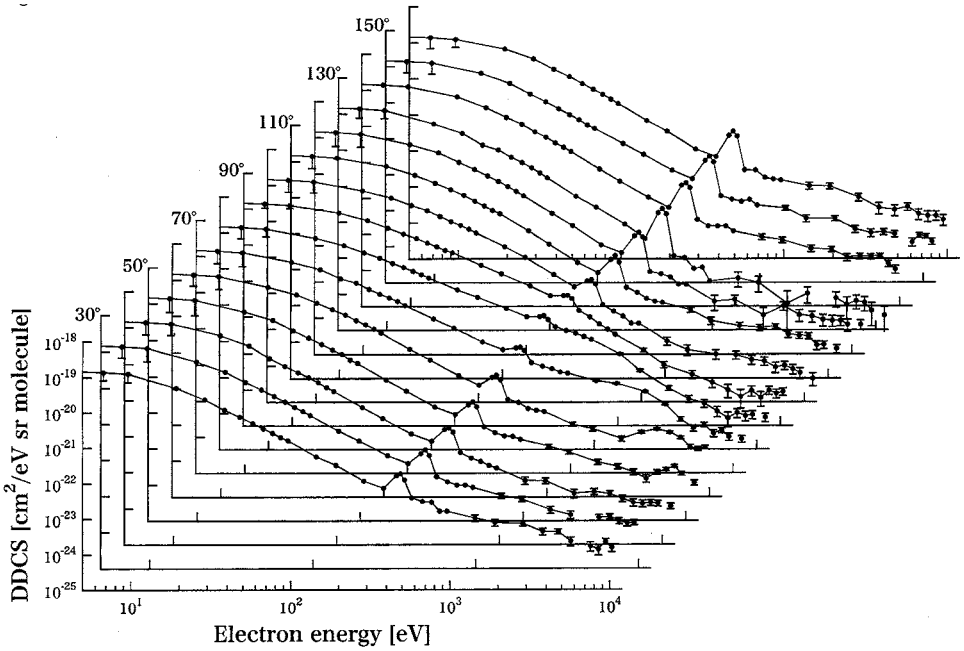

FIG. 2. DDCS's of secondary electrons (20–12 000 eV and 20°–160°) produced in the collision of 10.0-MeV/u He^{2+} ions with H_2O molecules. The data points with energies of 1–10 eV are not indicated, because their values are not reliable, due to the effects of the residual magnetic field.

surement with 10.0 MeV/u, the *K-LL* Auger peak was carefully found and systematically measured at exactly the same energy points at all angles, resulting in a relatively clear appearance of the Auger peak, compared to the case of 6.0 MeV/u, in which this process was not perfectly performed. In the energy range lower than 20–30 eV, isotropic emission was observed, which was due to soft collisions. At angles smaller than 90°, binary encounter peaks were observed at energies slightly smaller than the calculations on stationary-free electrons. BE peaks are produced through elastic collisions between incident ions and target electrons, in which the scattering angles and electron energies can be determined from the formulas of both momentum and energy conservation between incident ions and stationary-free electrons.

In the intermediate-energy region between soft collisions and BE peaks (high-energy region), the 90° emission should be predominant, as explained in Appendix A. Since the effects of the momentum spread are actually added to this emission, analyses of the DDCS spectrum generally require an approach based on perturbation theory. In this energy region, the single-center effect no longer plays an important role. Particularly, for a high-Z target, where Z is the target nuclear charge, the momentum spread is large and can affect the electron emission even at backward angles, such as 160°. For high-energy projectiles, BE peaks are observed in the high-energy region and are far from the soft-collision region. Therefore, the DDCS spectrum depends strongly on both the energy of incident ions and the Z values of the target. These simple predictions can be clearly observed in our DDCS data of 6.0- and 10.0-MeV/u He^{2+} ions on a high-Z target (H_2O): a wide range (20–200 eV) of intermediate-energy region, broad BE peaks at the angles $<90°$, and a wide angular distribution, such as 160°.

In the following, we try to estimate the limitation of the classical approach and the necessity of introducing advanced theories, based on a comparison between Toburen's data and ours, regarding the same projectile (He^{2+}) on the same target (H_2O) with different projectile energies.

B. Angular distribution

Figures 3 and 4 show the angular distributions at several electron energies, in which the following features are observed: first, they are nearly isotropic for electron energies of $\leqslant$20 eV and are accompanied by a slightly symmetric distribution around 90°; second, for electron energies of ~20–200 eV, this symmetric property becomes clear; in other words, the 90° emission is predominant; third, as the electron energy increases at $\geqslant$200 eV, this peak is gradually displaced to the forward angles, due mainly to the effects by BE electrons.

In the following subsections, the discussions are separately presented in three different energy regions, such as soft collision (low), BE peaks (high), and between these two regions (intermediate).

1. Low-energy electrons

a. Our data (6.0- and 10.0-MeV/u He^{2+} ions on water vapor). Nearly isotropic emissions can be seen in both Figs. 3 and 4. In such a low-energy region, the single-center (target nuclear-charge) effect plays an important role. Electrons initially move toward 90°, and this transversal direction should soon be relaxed due to the strong Coulomb force of the target nuclear charge, thus showing an isotropic distribution. This is an essence in soft collisions, leading to a broad angular distribution at around 90°. A similar distribution can also be seen in Toburen's data of 20-eV electrons ejected from xenon in collisions of 20-MeV protons [23], in which the effects by a high-Z target are observed.

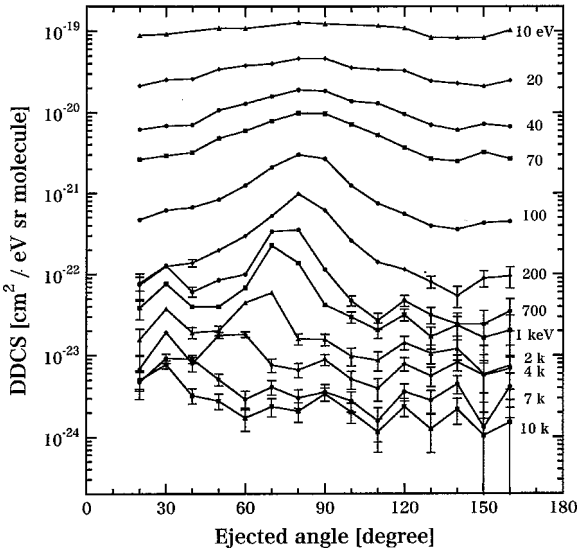

FIG. 3. Angular distributions of DDCS's at different electron energies in the collision of 6.0-MeV/u He^{2+} ions with H_2O molecules. At energies lower than 1 keV, error bars are not indicated, except for a few data points, because most of them are smaller than the size of symbols.

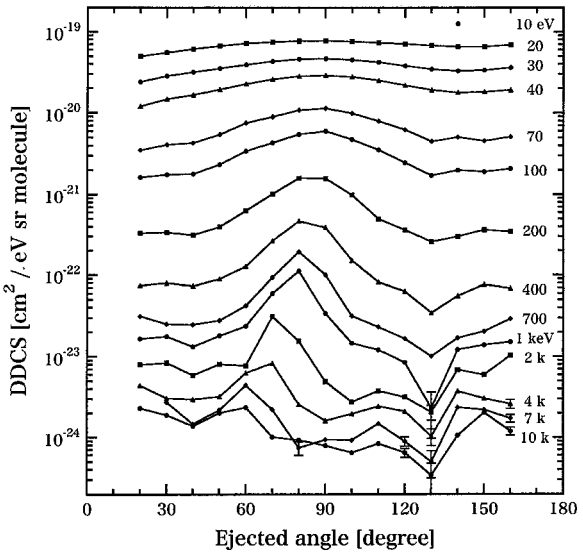

FIG. 4. Angular distribution of DDCS's at different electron energies in the collision of 10.0-MeV/u He^{2+} ions with H_2O molecules. At energies lower than 1 keV, error bars are not indicated, except for a few data points, because most of them are smaller than the size of symbols.

b. Toburen's data (0.2–0.5-MeV/u He^{2+} ions on water vapor). Isotropic distributions cannot be observed, and a small decrease in the emission with an increase in the angle can be seen; particularly, the emission at the forward angle is predominant. These characteristics should be attributed only to the difference in the energy of incident ions between our and Toburen's cases, for which there are two possible explanations. One is the effect by BE peaks; when the energy of incident ions is low in Toburen's case, BE peaks appear at relatively low energy. For example, at an angle of 80°, 0.5-MeV/u He^{2+} ions produce a BE peak at only 31 eV, and its energy spread should be large due to the high-Z target, suggesting a symmetric distribution around 90°, but not an isotropic distribution, even in such a low-energy region. The other one is the two-center effect (target and projectile); when the energy of incident ions is low, the ejected electrons are affected by the Coulomb force of the projectile nuclear charge for a long time, resulting in a displacement of the previous broad peak to the forward angles. It seems to be possible to quantitatively describe this subject through an approach by taking quantum mechanisms into account.

c. Fano plot. A comparison of the experimental data with a theoretical model using a dipole approximation can be made. Kim [24] and Inokuti [25] outlined corresponding calculations and showed that ionization processes occurring with large impact parameters (small momentum transfer) can be treated similar to photoionization processes. In such a case of large impact parameters, the momentum transfer to the atomic electrons is nearly perpendicular to the path of the projectile. Using the first Born approximation, it can be shown that the product of the measured cross section (σ) and the projectile energy (T) for a given electron energy (W) and ejection angle (θ) is plotted as a function of $\ln T$, which is a well-known Fano plot and should be a straight line:

$$\frac{d^2\sigma(W \to 0, \theta)}{dW d\Omega} \propto \frac{\ln T}{T}. \tag{2}$$

In addition, it can be shown that

$$A_{ew}(90° - \alpha) = A_{ew}(90° + \alpha), \tag{3}$$

where $A_{ew}(\theta)$ is proportional to the dipole oscillator strength as a function of θ and α is some arbitrary angles. As a result, a Fano plot for secondary electrons with $\theta=(90°-\alpha)$ should be parallel to that with $\theta=(90°+\alpha)$. Based on this theory, Figs. 5(a)–5(e) are introduced concerning 70° and 110° ($\alpha=20°$), which show the relations between $\sigma(W,\theta)T$ and $\ln T$ at different electron energies of 10–50 eV for several different projectile energies of 0.2–10.0 MeV/u. T is the kinetic energy of electrons having the same velocity as a projectile. Both the vertical and horizontal axes are normalized by using the Bohr radius a_0 ($=5.29\times10^{-9}$ cm) and the Rydberg energy R (=13.6 eV). Figures 5(c)–5(e) ⩾30 eV clearly show the following two characteristics: one is good linearity, as can be seen at 110° between 0.2 and 6.0 MeV/u; $\ln(T/R)=2.1-5.5$, which implies that there is a good consistency between ours and Toburen's data. In the case of 10-MeV/u He^{2+} ions [$\ln(T/R)=6.0$], the low-energy electrons were not precisely measured, due to the residual magnetic field; the other one is that such a "parallel property" becomes clear with an increase of the electron energies and projectile energies, which is particularly observed in the Fig. 5(e) for ⩾6.0 MeV/u, though such a parallel property cannot be seen for ⩽0.5 MeV/u, showing that the first Born approximation does not hold. This is because the two-center effects are not negligible, resulting in a significant yield in the forward direction. Equation (2), the first Born approximation, takes the single-center effects into account, but not two-center effects. On the contrary, at high projectile energy (our case), the parallel property is clearly observed between both lines, suggesting that the first Born approximation is valid. In such a high-projectile-velocity region, the single-center effects still play an important role in the low-energy region.

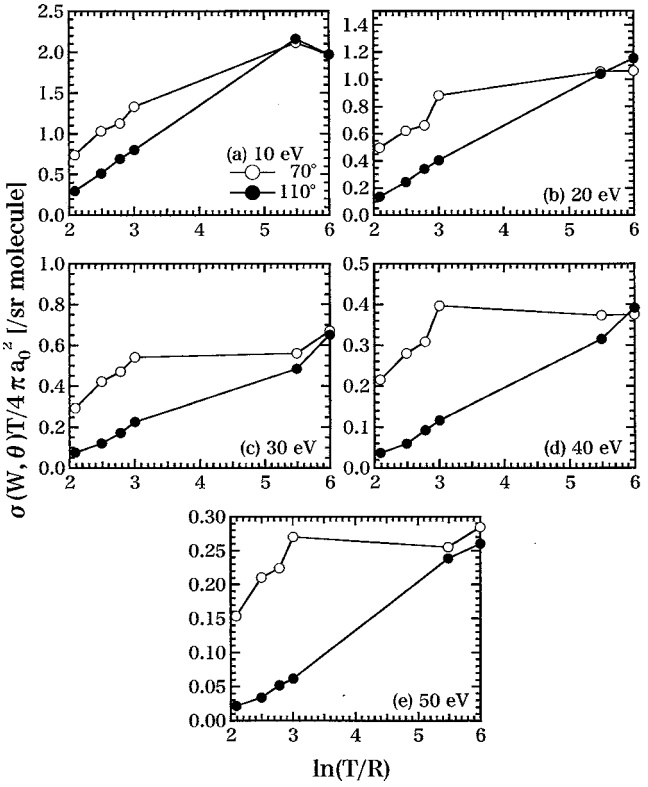

FIG. 5. Fano plots for secondary electrons with energies of 10–50 eV at the emission angles of 70° and 110°, which are produced in the collision of 0.2–0.5-MeV/u He^{2+} [1] and 6.0–10.0-MeV/u He^{2+} ions on water vapor. The incident He^{2+} energy T is expressed in units of the equivalent velocity of an electron energy. Both the vertical and horizontal axes are normalized by using the Bohr radius a_0($=5.29\times10^{-9}$ cm) and the Rydberg energy R(=13.6 eV).

2. Intermediate-energy electrons

a. Our data. In the cases of 6.0- and 10.0-MeV/u He^{2+} ions, the energy range of 20–200 eV seems to be included in this energy region, where the 90° emission is predominant and the above-mentioned symmetric property around 90° is also observed. These tendencies become clear with increases

TABLE I. Measured and calculated BE energies in the collision of 0.4–10.0-MeV/u He^{2+} ions with H_2O molecules. Calculations are made in the collision of projectiles with stationary-free electrons by taking the relativistic effects into account. Errors in BE shift are statistically produced in the process of fitting to a Gaussian. The estimated uncertainty in energies is on the order of ±2% which corresponds to ±200 eV for 10 keV. In our case (6.0 and 10.0 MeV/u), the measurement at ~12 keV was usually impossible due to the frequent sparks in the spectrometer. The evaluation at 80° was not made, because the peak was masked by the 90° component.

Angles (deg)	10	20	30	40	50	60	70
0.4-MeV/u He^{2+} ions by Toburen's work							
Calculation (eV)	851	774	658				
Measured (eV)	697	617	481				
BE shift (eV)	−154	−157	−177				
FWHM (eV)	349	257	255				
0.5-MeV/u He^{2+} ions by Toburen's work							
Calculation (eV)	1063	968	822				
Measured (eV)	904	815	637				
BE shift (eV)	−159	−153	−185				
FWHM (eV)	313	324	317				
6.0-MeV/u He^{2+} ions in this work							
Calculation (eV)			9865	7702	5411	3267	1526
Measured (eV)			8764	6994	4777	2800	1371
BE shift (eV)			−1101±75	−708±63	−634±82	−467±50	−155±23
FWHM (eV)			2114	1790	2269	1766	1317
10.0-MeV/u He^{2+} ions in this work							
Calculation (eV)			16441	12819	8992	5422	2530
Measured (eV)					8544	5195	2493
BE shift (eV)					−448±238	−227±42	−37±24
FWHM (eV)					2375	2913	1718

of electron energies. In this electron energy, the single-center effect does not play an important role, and the scattering angle of electrons is nearly perpendicular to the projectile injection axis when the impact parameter is large (see Appendix A), resulting in a large emission at 90°. In addition, these electrons have some momentum spread, thus showing a wide distribution of the BE peak so as to be observed even in the low-energy region. This reflects a nearly symmetric distribution at around 90°, leading to a large DDCS value, even in the backward angles.

As can be slightly seen in Fig. 1 in the case of a 6.0-MeV/u projectile, the BE peak energy at 80° is calculated to be 370 eV and is still high, compared to the low-energy electrons considered here, suggesting no effect on the angular distributions for electron energies lower than ~200 eV, but a possibility to produce symmetry distributions at around 90° in this energy region. However, this tendency cannot be seen in Toburen's data in the collision of 2.0-MeV protons with xenon; a possible explanation is that the corresponding BE peak energy is relatively low (120 eV), which may have enhanced the forward component.

b. Toburen's data. As previously mentioned, this region cannot exist due to the small energy of incident ions; even for 0.5-MeV/u He^{2+} ions, the corresponding energy is on the order of 20–30 eV. It is noted that there can be seen a small BE peak at ~80°; hereafter, the emission decreases monotonically with increasing angles.

3. High-energy electrons

a. General features in our data. In the cases of 6.0- and 10.0-MeV/u He^{2+} ions, the energy range of $\gtrsim$200 eV is included. In this energy region, it has been widely accepted that the two-center effect plays an important role in the angular distributions, as well as the BE peaks.

Figures 3 and 4 show the following two general features: first, the energies of the BE peaks were gradually displaced from ~90° to the forward angles with the electron energies increasing; second, for backward angles of $\geqslant$130°, the cross sections were unexpectedly large, and this tendency also becomes clear with the electron energies increasing. Concerning the BE peaks, the observed peak energies and their FWHM values were compared with calculations, including relativistic corrections (see Appendix B 1) between our data (30°–70°, 6.0 and 10.0 MeV/u) and Toburen's data (10°–30°, 0.4 and 0.5 MeV/u), of which the results are summarized in Table I. In both experiments, the peak energies were observed to be smaller than the calculated values; the difference (BE shift to the lower energies) decreases with the angles increasing in our data, while it is nearly constant in Toburen's data. The observed FWHM values in the our data

are much larger than those seen in Toburen's data. In the following, the BE shift and the FWHM of BE peaks are discussed, as well as the unexpectedly large emission at angles larger than 130°.

b. BE shift. There can be three main factors causing BE shifts to lower energies: the momentum distribution of bound electrons to a target nucleus, single- and two-center effects, and Fermi-shuttle acceleration, as well as combinations of these effects. The free-electron Born approximation shows that the BE energies are smaller than those calculated for stationary free electrons by $2E_B$ [16,26], where E_B is the binding energy and is on the order of ~10 eV for H_2O molecules; however, this contribution is basically small and has no dependence on the angles, thus making it impossible to describe the observed large BE shift, such as ~1 keV at 30° in the case of 6.0 MeV/u (see Table I).

The BE shift due to the single-center effects is considered in the following. To make this explanation simple, we try to consider the BE collision by neglecting the momentum spread of the bound electrons. If the impact parameter b is given, the scattering angle θ and the velocity v of an electron are uniquely determined, respectively; when b is large, θ becomes large and v small. In the measurement, part of electrons with impact parameter $b\pm\Delta b$ ($\theta\pm\Delta\theta$) are deflected to θ due to the single-center effects and are simultaneously observed at a certain angle θ, where the low-energy electrons with $b+\Delta b$ ($v-\Delta v$) act as producing a negative shift and the high-energy electrons with $b-\Delta b$ ($v+\Delta v$) a positive shift. With an increase of θ, the former component generally becomes small and the latter large, leading to a reduction of the negative shift. In the extreme case at $\theta=0$ ($b=0$), there is only a negative shift, and it reaches the maximum. From this point of view, the BE shift should have a dependence on the angles. Although a quantitative consideration has not yet been made, this tendency is consistent with our data in Table I.

The two-center effects were described by Fainstein *et al.* [16] and Hidmi *et al.* [27], in which the corresponding BE shift was also reported, though the details are still an open question. The latter two contributions seem to be relatively larger than the first one ($\sim 2E_B$), though still being insufficient to well explain the observed large BE shift.

Recently, Lanzanó *et al.* reported two important pieces of evidences using high-energy projectiles: the large BE shift and the large FWHM of BE peaks obtained in the collision of 45-MeV/u Ni ions with different solid (foil) targets [28,29]. Concerning the former, he showed that the BE shift becomes large with the projectile energy increasing, which is consistent with our results. As can also be seen in Table I, the FWHM values of BE peaks in our data are distributed in 1.3–2.9 keV and are much larger than those of Toburen's data (153–185 eV). It has generally been accepted that the FWHM value reflects the momentum distributions of bound electrons (Compton profile). The FWHM values should thus be basically similar for the same target, such as our and Toburen's cases (water vapor); however, the obtained data show a quite different tendency. One can thus conclude that the observed large difference cannot be explained only by simple two-body relativistic kinematics, suggesting an additional mechanism characterized by the fast and low-Z projectiles. As was also proposed by Lanzanó *et al.*, the most probable contribution seems to be related to Fermi-shuttle acceleration, which is discussed in Sec. IV C.

c. Unexpectedly large emission at the angles larger than 130°. This unexpected increase is too large to be explained only by the Compton profile. In addition, Toburen's data by 0.2–0.5 MeV/u He^{2+} [1] on the same target also show a small enhancement at 110° and 125° (no data at >130°), thus also suggesting an unexpected phenomenon, which cannot be predicted from a simple two-body collision theory. As discussed in Sec. IV C (SDCS), the effect of the Fermi-shuttle acceleration seems most probable.

The large yield of high-energy electrons in the backward angles can be described in principle by the backscattered components produced through the P-T processes by Fermi-shuttle acceleration, where P and T denote the scattering of electrons by the projectile and target nucleus, respectively. As mentioned in the following, the attraction of target electrons to a projectile can occur in the Fermi-shuttle acceleration. In our experiment, the effect of attraction is weak, due to a low Z (=2) and a high-velocity projectile. Before the first P process, there can be a mixture of electrons with and without attraction. In the 0.1–1.1- (3.5-) keV region in Figs. 3 and 4, the electron emission at ~90° is dominant; however, a small part has already been attracted toward the projectile, before being scattered with a velocity of $\sim 2V$ through the P-T processes, and another small part is simply scattered in the forward angles with velocities of $2V\cos\theta$. Figures 4 and 5 show the final results after these processes. The latter case is the well-known BE electron emission, in which the dominant component appears in forward angles with small deflection. Even if a small amount of attracted electrons are included, it cannot be distinguished in the angular distribution having a symmetric distribution around the BE angles due to the momentum spread of bound electrons. Meanwhile, at backward angles, the backscattered components can generate a pronounced peak due to backscattering by an attractive screened Coulomb potential through the T process, of which the mechanism was well described by Jakas [30]. Detailed descriptions of Fermi-shuttle acceleration at high energies are presented in Ref. 31.

d. Toburen's data. In the case of 0.5-MeV/u He^{2+} ions, the equivalent electron energy corresponds to $\gtrsim$30 eV. The emission is predominant at angles smaller than where the predicted BE peaks occur, resulting in broad BE peaks. Such a high yield at forward angles seems to be attributed to two-center effects. On the other hand, the emission at angles larger than the BE peaks is similar to our data. As can be seen in Table I, the observed BE peaks energies are smaller than the calculated by 153–185 eV at 10°–30°, which are also due mainly to the single- and two-center effects, as well as the binding energy. The FWHM values of the BE peaks are on the order of 300 eV, as shown in Table I.

The observed tendency in BE shifts between our and To-

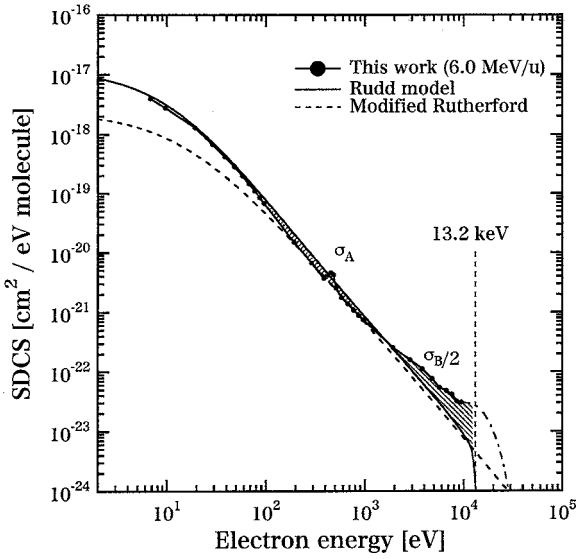

FIG. 6. Energy spectra of SDCS deduced from the experimental DDCS values obtained in the collisions of 6.0-MeV/u He^{2+} ions with H_2O molecules. The solid and dashed lines show the Rudd model and the modified relativistic Rutherford cross section, respectively. Comparing our SDCS values to the Rudd model, σ_A and σ_B are defined at $\sim$0.1–1.1 keV and at $\geqslant$1.1 keV; the former corresponds to the reduction and the latter to the enhancement. When V denotes the projectile velocity, σ_B is assumed to have a symmetric distribution around $2V$ (13.2 keV).

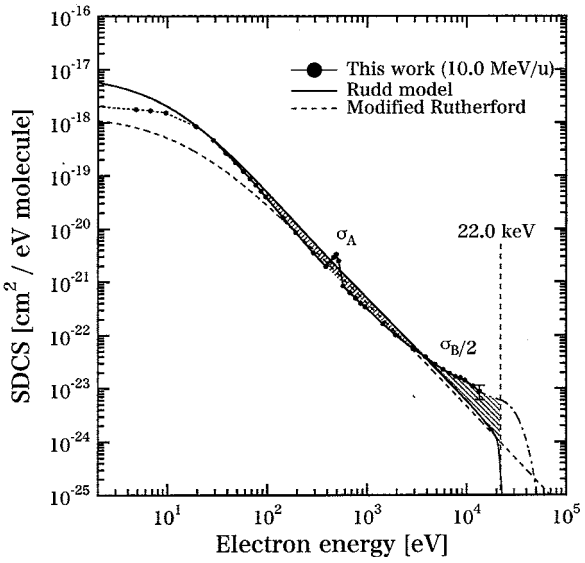

FIG. 7. Energy spectra of SDCS deduced from the experimental DDCS values obtained both in the collisions of 10.0-MeV/u He^{2+} ions with H_2O molecules. The solid and dashed lines show the Rudd model and the modified relativistic Rutherford cross section, respectively. Since the DDCS value at 14 keV was measured only at 150°, the SDCS value here was simply estimated in a way that the shape of angular distribution would equal to that at 12 keV, thus showing a large uncertainty of ±30%. Comparing our SDCS values to the Rudd model, σ_A and σ_B are defined at $\sim$0.1–3.5 keV and $\geqslant$3.5 keV; the former corresponds to the reduction and the latter to the enhancement. When V denotes the projectile velocity, σ_B is assumed to have a symmetric distribution around $2V$ (22.0 keV).

buren's data, however, does not agree with the recent consideration by Lee *et al.* [32]. They showed that the BE shift becomes smaller at higher projectile energies by the measurement of BE electrons at 0° in collisions of several of 1–2-MeV/u heavy ions with H_2 and He targets. Clear explanations for the observed difference in the BE shift between our and Toburen's data have not yet been obtained.

C. SDCS

Figures 6 and 7 show the SDCS spectra obtained from the measured DDCS values by integration with respect to the ejected angle. The obtained SDCS values were compared with the modified relativistic Rutherford cross section and the Rudd model [6]; the former takes account of the relativistic correction and the binding energy of an electron ejected from each subshell of a water molecule (see Appendix B 2), and the latter is based on both the molecular promotion model applied to electron emission by low-energy ions and the classical binary-encounter approximation at high energies, so as to agree with the Bethe theory on ionization. Although the Rudd model was basically derived from experiments with protons having energies of 5–5000 keV, it has been widely accepted to be applicable to other bare projectiles by Z^2 scaling.

Figure 8 shows our SDCS values normalized by the Rudd model, of which the discrepancies are discussed separately in the different energy regions of $\leqslant$100 eV and $>$100 eV; a value of 100 eV is the energy where the difference between the experimental curve and the Rudd model becomes clear.

1. ≤100 eV

In the energy range of 20–100 eV, there is a good agreement with the model of Rudd in the case of 6.0-MeV/u He^{2+} ions. As can be seen in Fig. 8 at $\leqslant$10 eV for 10.0-MeV/u He^{2+} ions, the discrepancy between our data and Rudd model is much larger than the case for 6.0-MeV/u He^{2+} ions; we believe this is due to a previously mentioned unwanted increase in the residual magnetic field.

2. >100 eV

Both in the 6.0- and 10.0-MeV/u cases, the discrepancies are clearly demonstrated, mainly in two different energy regions 0.1–1.1 (3.5) keV and $\geqslant$1.1 (3.5) keV, respectively. In the former region, there are meaningful reductions by 26% (41%) at the maximum in $\sim$400 (600) eV. In the latter region, the discrepancies reach a factor of $\sim$3 at the maximum in 6.0 MeV/u and $\sim$2 at maximum in 10.0 MeV/u at around 10 keV. The primary reasons are considered in the following.

First, in this energy region, the two-center electron emission (TCEE) should play a dominant role in producing secondary electrons. Particularly, in high-Z projectiles, TCEE should occur at wide angles due to the strong Coulomb force of projectiles, which suggests that a simple Z^2 scaling of the Rudd model cannot be easily used to describe the experimental data for bare projectiles with $Z\geqslant 2$; hereafter, some im-

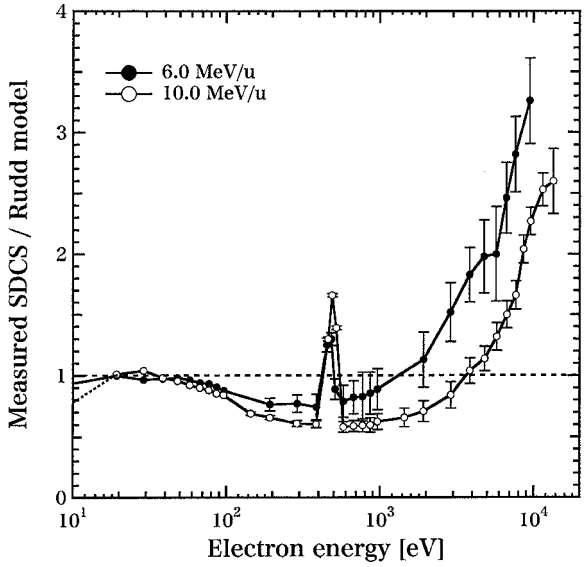

FIG. 8. Two SDCS curves deduced from the DDCS values obtained both in the collisions of 6.0- (●) and 10.0- (○) MeV/u He^{2+} ions with H_2O molecules, which are normalized by those of the Rudd model. The error bars show the corresponding statistical errors, to which the uncertainty (systematic error) of ±13% should be added (not indicated here). The values at ⩽10 eV for 10.0 MeV/u are considerably small, due to the effects of the residual magnetic field.

provements seem to be necessary regarding the Z dependence in the present Rudd model.

Second, part of discrepancies between the Z^2-scaling law and the measured data can generally be described by the well-known Barkas effect. This $L_1(\beta)$ is one of correction factors for the difference from the first Born approximation (Z^2 dependence) in the stopping-power formula by Bethe; details of this effect were theoretically [33] and experimentally [34] studied. Taking this effect into account, the ratio of the stopping power for He^{2+} to that for a proton of the same velocity is not exactly equal to 4. It is, however, considerably small for a projectile with a large velocity, such as our case; the effect is proportional to Z/V^3 [33], where Z is the nuclear charge of the target atom and V the velocity of the incident ion, and is meaningfully observed for projectile energies lower than several hundred keV/u. As a result, this effect cannot explain such a large discrepancy observed in our data.

Third, the large discrepancy at ⩾1.1 (3.5) keV suggests the emission of electrons having velocities higher than $2V$ (13.2 and 22.0 keV), where V is the projectile velocity and corresponds to an electron energy of 3.27 (5.45) keV. Such high-energy electrons cannot be predicted from a simple two-body collision theory. The effect of the Fermi-shuttle acceleration seems most probable. Since this phenomenon is basically accompanied by an acceleration mechanism regarding the electron energy, it should somewhat affect the energy spectrum (SDCS) of observed electrons. One can predict that part of electrons are accelerated through Fermi-shuttle acceleration process, resulting in a reduction in this energy region and a considerable increase in the high-energy region (≳3 keV).

In order to consider the origin of such high-energy electrons, an attempt was made to evaluate the amount of reduction at 0.1–1.1 (3.5) keV and increase at 1.1– (3.5–) 13.2 (22.0) keV. In both cases of 6.0 and 10.0 MeV/u, the reduction becomes clear at ⩾0.1 keV, and the experimental value is equal to the Rudd model at 1.1 and 3.5 keV, respectively. Here, we define the partial cross sections σ_A and σ_B corresponding to the former reduction and the latter increase. As can be seen in the case of 6.0 MeV/u (Fig. 6), the discrepancy at 1.1–13.2 keV is quite large and an ambiguity in the σ_B value is not greatly affected by the systematic error in the SDCS values. Therefore, the value of $\sigma_B/2$ was first calculated to be 3.56×10^{-19} cm^2, where σ_B is assumed to have a symmetric distribution at around 13.2 keV ($2V$), since it is due mainly to the momentum spread of orbital electrons; in this calculation, the SDCS values between 10 and 13.2 keV were extrapolated, since they were not measured due to sparks. Second, the lower limit in the integration region for σ_A was determined, so as to satisfy $\sigma_A=\sigma_B$; the lower limit was found to be 103 eV, which is quite consistent with the previous observation that the reduction becomes clear at ⩾0.1 keV, showing σ_A to be on the order of 7.1×10^{-19} cm^2. In the same way for 10.0 MeV/u (Fig. 7), σ_B was calculated to be 4.5×10^{-19} cm^2 between 3.5 and 22.0 keV and the lower limit to be 370 eV. Although this limit is much greater than 100 eV, the tendency is similar to the case of the 6.0 MeV/u. In addition, there could be higher order components at ~$4V$ or more through Fermi-shuttle acceleration, but we can assume their yields are negligibly small. It is therefore highly likely that the unexpectedly high yield of high-energy electrons comes mainly from the electrons in the energy range of 0.1–1.1 (3.5) keV.

In order to consider the acceleration mechanism of electrons, it is necessary to introduce the idea of "attraction" of electrons toward the projectile nuclear charge; part of the bound electrons belong to the target core, which have relatively small impact parameters corresponding to those the above-mentioned 0.1–1.1- (3.5-) keV electrons should have, and are directly attracted toward the projectile, before being scattered by the projectile. The attraction causes an acceleration of bound electrons to ~$2V$ through the Fermi-shuttle acceleration process, which was theoretically explained by Reinhold *et al.* [22]. The effect in the attraction of electrons toward a projectile strongly reduces the impact parameter (b), resulting in a large momentum transfer to electrons.

Another attempt was made to compare the total ionization cross sections (TICS) with the calculations by theoretical models, in order to support the above evaluation. By integrating the SDCS curves of 6.0- and 10.0-MeV/u He^{2+} ions, the TICS values were calculated to be 0.99 and 0.63 $\times10^{-16}$ cm^2, respectively, in which the Rudd model was used in the low-energy region (⩽20 eV) and the experimental values in the other energy regions. These TICS values are quite consistent with two calculations. One is made by the LOSS [35] code and gives the values of 0.96 and 0.61 $\times10^{-16}$ cm^2. The LOSS code is based on the first Born approximation for ionization cross sections with the use of accurate radial wave functions of the ionized electrons and the atomic structure of the perturbing atom. The other calcula-

tion results in 0.95 and 0.62×10^{-16} cm^2 followed from the KURBUC code and based on a Monte Carlo track simulation [36], thus strongly supporting the previous suggestion. Therefore, the total electron emission is described by the Rudd model, in which part of the electrons, corresponding to ~0.7% of the TICS value, are accelerated to high energies in the collision of 6.0–10.0-MeV/u He^{2+} ions on water vapor.

V. CONCLUSION

DDCS data of electron emission with 6.0- and 10.0 -MeV/u He^{2+} ions on water vapor were presented and analyzed. A Fano plot in the low-energy (soft collision) region showed a very good consistency between our and Toburen's data with 0.2–0.5-MeV/u He^{2+} ions on the same target, implying that the first Born approximation holds well in our case.

Concerning the angular distributions, both our data at ~20–200 eV and most of Toburen's data can be qualitatively explained by the Rutherford cross section and two-center effects, suggesting the necessity of new models while taking the two-center effects fully into account, which may also be helpful to well explain the discrepancy (−41%) in the ~600-eV region in SDCS between ours and the Rudd model, as well as the large BE shift and wide FWHM values of the BE peaks.

Unexpectedly large DDCS values were observed at the backward angles, particularly >130° in the data of 10.0 -MeV/u He^{2+} ions, due to elastic backscattering by the target nucleus. This phenomenon should also be related to a pronounced large yield in SDCS both at ~10 keV, which can reasonably be explained by the Fermi-shuttle acceleration mechanism.

ACKNOWLEDGMENTS

The authors are very grateful to Dr. L.H. Toburen (ECU) for sending us his experimental data in the collision of 0.2–0.5-MeV/u He^{2+} ions on water vapor. We are also grateful to Dr. H. Honma for his great efforts to provide a well-reproducible beam from the cyclotron and to Dr. M. Inokuti (ANL), Dr. M. Kanazawa (NIRS), and Dr. T. Tomitani (NIRS) for fruitful discussions on atomic physics. The experiments were carried out at the NIRS isochronous cyclotron facility, as a subprogram of Physics-009 in the Research Project with Heavy Ions at NIRS-HIMAC.

APPENDIX A: RUTHERFORD CROSS SECTION IN THE LABORATORY FRAME

When an incident ion A with mass m_A, charge $+ze$, and velocity v_A collides with a rest particle (electron) B with a mass m_B and charge $-e$, the relation between the scattering angle θ between the laboratory (Lab) frame and the center-of-mass (c.m.) frame is expressed as follows:

$$\tan\theta_{\mathrm{Lab}A}=\frac{m_A\sin\theta_{\mathrm{c.m.}}}{m_A+m_B\cos\theta_{\mathrm{c.m.}}},\tag{A1}$$

$$\theta_{\mathrm{Lab}B}=\frac{\pi-\theta_{\mathrm{c.m.}}}{2},\tag{A2}$$

where $\theta_{\mathrm{Lab}A}$ and $\theta_{\mathrm{Lab}B}$ are the scattering angles of A and B in the laboratory frame, respectively, and $\theta_{\mathrm{c.m.}}$ is the scattering angle in the c.m. frame. By using Eq. (A2), the velocity (v_B) of B is given as

$$v_B=\frac{2m_Av_A}{m_A+m_B}\sin\frac{\theta_{\mathrm{c.m.}}}{2}.\tag{A3}$$

The well-known Rutherford scattering formula in the c.m. frame is given by

$$\frac{d\sigma_{\mathrm{c.m.}}}{d\Omega_{\mathrm{c.m.}}}=\left(\frac{ze^2}{4\pi\varepsilon_0 2mv^2}\right)^2\sin^{-4}\left(\frac{\theta_{\mathrm{c.m.}}}{2}\right),\tag{A4}$$

where ε_0 is a dielectric constant in vacuum, m is the reduced mass [$=m_Am_B/(m_A+m_B)$], and v the relative velocity. The relation between θ and the solid angle Ω is generally given by

$$d\Omega=2\pi\sin\theta\,d\theta.\tag{A5}$$

Taking the condition $m_A\gg m_B$ into account, the scattering cross section for particle B in the laboratory frame can be rewritten as

$$\frac{d\sigma_{\mathrm{Lab}B}}{d\Omega_{\mathrm{Lab}B}}=\left(\frac{ze^2}{4\pi\varepsilon_0 m_Bv_A^2}\right)^2\cos^{-3}\theta_{\mathrm{Lab}B}.\tag{A6}$$

When considering the collisions between an incident ion and stationary-free unbounded electrons, each collision can be treated as a two-body problem. In this case, $\theta_{\mathrm{Lab}B}$ and v_B after the collision are uniquely determined by v_A and the impact parameter b, of which the calculated result corresponds to the well-known BE peak. When b is large, $\theta_{\mathrm{Lab}B}$ also becomes large and v_B small, though the maximum $\theta_{\mathrm{Lab}B}$ is limited by $\pi/2$, as can be seen from Eq. (A2). In this case the electrons with energies lower than the BE-peak energy at ~80° should be basically scattered toward ~90°; these are the main components in Eq. (A6). The orbital electrons bound to a nucleus have some momentum spread, thus showing a wider distribution of BE peak particularly for high-Z targets and thus giving a significant contribution in the measured DDCS at the backward angles. Symmetric distributions around 90° can thus be predicted, and these are consistent with a dipole approximation, which is quite useful for considering the scattering with a large impact parameter.

APPENDIX B: RELATIVISTIC CORRECTION

In our experiments, the β value (ratio of particle velocity to the light speed) of the projectile exceeds 0.1 and the maximum energy (~12–14 keV) of electrons reaches 0.2, suggesting the necessity of relativistic corrections in the two-body collision processes, such as the Rutherford cross section and the binary encounter collision, regarding the mass of the projectiles and electrons.

1. Binary encounter peak

When E, P, and m_0 are defined as the total energy, the relativistic momentum, and the rest mass of a particle, re-

spectively, the following equation generally holds:

$$\frac{E^2}{c^2} - P^2 = m_0^2 c^2, \tag{B1}$$

where c is the light velocity. The relativistic kinetic energy T is given as

$$E = T + m_0 c^2. \tag{B2}$$

By using Eqs. (B1) and (B2), P can be rewritten as

$$P = \sqrt{\frac{T^2}{c^2} + 2m_0 T}. \tag{B3}$$

When an incident particle A having m_A and T_A collides with a rest particle B having m_B, the scattering angles $\theta_{\mathrm{Lab}A}$ and $\theta_{\mathrm{Lab}B}$ (for A and B) are given by both the momentum and energy conservation formulas, as follows:

$$\sqrt{\frac{T_A^2}{c^2} + 2m_A T_A} = \sqrt{\frac{T_B^2}{c^2} + 2m_B T_B}\cos\theta_{\mathrm{Lab}B} + \sqrt{\frac{T_A'^2}{c^2} + 2m_A T_A'}\cos\theta_{\mathrm{Lab}A}, \tag{B4}$$

$$0 = \sqrt{\frac{T_B^2}{c^2} + 2m_B T_B}\sin\theta_{\mathrm{Lab}B} - \sqrt{\frac{T_A'^2}{c^2} + 2m_A T_A'}\sin\theta_{\mathrm{Lab}A}, \tag{B5}$$

$$(T_A + m_A c^2) + m_B c^2 = (T_B + m_B c^2) + (T_A' + m_A c^2), \tag{B6}$$

where T_B and T_A' are the kinetic energy of A and B after the collision, respectively. In the above three equations, $\theta_{\mathrm{Lab}A}$ and T_A' can be eliminated; then, θ is expressed as

$$\cos\theta_{\mathrm{Lab}B} = \frac{m_A(1 + T_A/m_A c^2) + m_B}{\sqrt{m_A m_B(2 + T_A/m_A c^2)(2 + T_B/m_B c^2)}}\sqrt{\frac{T_B}{T_A}}. \tag{B7}$$

On the other hand, in the nonrelativistic region, the following relation generally holds:

$$\frac{T_A}{m_A c^2}, \frac{T_B}{m_B c^2} \ll 1. \tag{B8}$$

Under this condition, Eq. (B7) can be rewritten as

$$\cos\theta_{\mathrm{Lab}B} = \frac{m_A + m_B}{2\sqrt{m_A m_B}}\sqrt{\frac{T_B}{T_A}}. \tag{B9}$$

This expression gives the nonrelativistic binary encounter (BE) angles. The difference in the calculated energy of BE electrons between with and without relativistic correction is about ~1%.

2. Rutherford cross section

In the early work by McKinley and Feshback [37], the relativistic Rutherford cross section was approximately obtained as

$$\frac{d\sigma_{\mathrm{rel}}}{d\Omega_{\mathrm{c.m.}}} = (1-\beta^2)\left[1 - \beta^2\sin^2\left(\frac{\theta_{\mathrm{c.m.}}}{2}\right) + \pi\alpha\beta\sin\frac{\theta_{\mathrm{c.m.}}}{2}\left(1 - \sin\frac{\theta_{\mathrm{c.m.}}}{2}\right)\right]\frac{d\sigma_{\mathrm{nonrel}}}{d\Omega_{\mathrm{c.m.}}}, \tag{B10}$$

where α and β are defined as follows, respectively:

$$\alpha = \frac{ze^2}{4\pi\varepsilon_0\hbar c} = \frac{z}{137}, \tag{B11}$$

$$\beta = \frac{v}{c}, \tag{B12}$$

in which $(1-\beta^2)$ is the Lorentz contraction factor and $d\sigma_{\mathrm{nonrel}}/d\Omega_{\mathrm{c.m.}}$ is the nonrelativistic Rutherford cross section, which is Eq. (A4).

When an incident ion A with mass m_A, charge $+ze$, and velocity v_A collides with a rest particle (electron) B with mass m_B and charge $-e$, the energy transfer (T) from particle A to B is given according to the following expression from Eq. (A3), where the kinetic energy of particle A is T_A $(=m_A v_A^2/2)$:

$$T = \frac{m_B v_B^2}{2} = \frac{4m^2}{m_A m_B}T_A\sin^2\left(\frac{\theta_{\mathrm{c.m.}}}{2}\right). \tag{B13}$$

Substituting Eq. (B13), its differential form, and Eq. (A5) by Eq. (B10), the following expression can be obtained:

$$\frac{d\sigma_{\mathrm{rel}}}{dT} = \frac{\pi(ze^2/4\pi\varepsilon_0)^2}{(1-\beta^2)(m_B/m_A)T_A T^2}\left[1 - \beta^2\frac{T}{T_{\max}} + \pi\alpha\beta\left\{\sqrt{\frac{T}{T_{\max}}} - \frac{T}{T_{\max}}\right\}\right], \tag{B14}$$

where

$$T_{\max} = \frac{4m^2}{m_A m_B}T_A. \tag{B15}$$

When Eq. (B14) is rewritten using the Bohr radius a_0 and Rydberg energy R $(=e^2/8\pi\varepsilon_0 a_0)$ by taking account of the binding energy E_{bj} of orbital electrons j in a molecule, the differential cross section of ionized electrons with a kinetic energy of W is expressed as

$$\frac{d\sigma_{\mathrm{rel}}}{dW} = \frac{4\pi a_0^2 z^2\left[1 - \beta^2\frac{T}{T_{\max}} + \pi\alpha\beta\left\{\sqrt{\frac{T}{T_{\max}}} - \frac{T}{T_{\max}}\right\}\right]}{(1-\beta^2)(m_B/m_A)T_A} \times\sum_j N_j\left(\frac{R}{W + E_{bj}}\right)^2, \tag{B16}$$

where N_j is the number of electrons included in orbit j and the summation is carried out for all orbits in a molecule. Since Eq. (B13) is obtained under the nonrelativistic-process, Eq. (B16) does not give a perfect relativistic form; however, it can be used for $\beta \lesssim 0.2$ with a sufficiently good approximation.

Actually, Eq. (A6) may not precisely describe the angular distributions, due to the momentum spread of bound electrons, but Eq. (B16) well explains the energy spectrum, because the behaviors of increase and decrease in energy are canceled by each other, resulting in a good agreement regarding the SDCS between the measured and Rutherford cross sections.

3. Correction in the spectrometer

According to an increase in the mass of electrons due to relativistic effects, the required voltage for the deflector electrode in the energy spectrometer has to be increased to ensure electrons passing through a geometrically defined orbit, depending on their kinetic energies (W). It is thus necessary to correct the W values in all data (figures) involving cross sections.

The following equation shows the general kinematics of an electron with rest mass m_0 and charge $-e$ when it travels with velocity v in an electric field F:

$$\frac{d}{dt}\left(\frac{m_0 v_x}{\sqrt{1-(v/c)^2}}\right)=0, \quad \frac{d}{dt}\left(\frac{m_0 v_y}{\sqrt{1-(v/c)^2}}\right)=-eF, \tag{B17}$$

where

$$v^2 = v_x^2 + v_y^2. \tag{B18}$$

The position $\{x(t), y(t)\}$ of an electron can be analytically obtained as a function of time t by integrating Eq. (B17) under the incident velocity v_0 and the angles θ_0. When the separation of the entrance and exit slits is l, the trajectory of an electron can be expressed as

$$\frac{cm_0 v_0 \cos\theta_0}{eF\sqrt{1-(v_0/c)^2}} \ln\left(\frac{1+v_0 \sin\theta_0/c}{1-v_0 \sin\theta_0/c}\right) = l. \tag{B19}$$

Expanding this expression regarding the term including v_0/c into a power series, one obtains

$$\frac{1}{\sqrt{1-(v_0/c)^2}} = 1 + \frac{1}{2}\left(\frac{v_0}{c}\right)^2 + \frac{3}{8}\left(\frac{v_0}{c}\right)^3 + O\left(\frac{v_0}{c}\right)^4,$$

$$\ln\left(\frac{1+v_0 \sin\theta_0/c}{1-v_0 \sin\theta_0/c}\right) = 2\frac{v_0 \sin\theta_0}{c} + \frac{2}{3}\left(\frac{v_0 \sin\theta_0}{c}\right)^3 + O\left(\frac{v_0 \sin\theta_0}{c}\right)^4. \tag{B20}$$

Taking the condition of $v_0/c \ll 1$ into account for the second-order term, the following relation can be obtained:

$$\frac{m_0 v_0^2 \sin 2\theta_0}{eF}\left[1+\frac{1}{2}\left(\frac{v_0}{c}\right)^2\right] = l. \tag{B21}$$

By substituting $F=V/d$ (d is the separation of the parallel plates) and $\theta_0=45°$ into Eq. (B21) and by using W $(=m_0 {v_0}^2/2e)$ (eV), one obtains

$$W\left(1+\frac{W}{m_0 c^2/e}\right) = \frac{l}{2d}V. \tag{B22}$$

Neglecting the second-order term in Eq. (B22), one can obtain the well-known nonrelativistic form

$$W = \frac{l}{2d}V. \tag{B23}$$

The second term in Eq. (B21) corresponds to a correction factor by relativistic effects and is negligibly small at an energy of $\leqslant 1$ keV; it reaches $\sim 2.0\%$ at 10 keV. In our experimental setup, the corresponding parameters are $d = 15.0$ mm (separation of the parallel plates), $l = 40.0$ mm (slit separation) in our case.

[1] L. H. Toburen, W. E. Wilson, and R. J. Popowich, Radiat. Res. **82**, 27 (1980).

[2] T. Nakano, M. Suzuki, A. Abe, Y. Suzuki, S. Morita, J. Mizoe, S. Sato, T. Miyamoto, T. Kamada, H. Kato, and H. Tsujii, Cancer J. Sci. Am. **5**(6), 369 (1999).

[3] T. Kanai, M. Endo, S. Minohara, N. Miyahara, H. Koyama-ito, H. Tomura, N. Matsufuji, Y. Futami, A. Fukumura, T. Hiraoka, Y. Furusawa, K. Ando, M. Suzuki, F. Soga, and K. Kawachi, Int. J. Radiat. Oncol., Biol., Phys. **44**, 201 (1999).

[4] E. W. McDaniel, J. B. A. Mitchell, and M. E. Rudd, *Atomic Collisions: Heavy particle projectiles* (John Wiley & Sons, New York, 1993).

[5] N. Stolterfoht, R. D. DuBois, and R. D. Rivarola, *Electron Emission in Heavy Ion-Atom Collisions* (Springer, Berlin, 1997).

[6] M. E. Rudd, Y.-K. Kim, D. H. Madison, and T. J. Gay, Rev. Mod. Phys. **64**, 441 (1992).

[7] ICRU Report 55, Bethesda, Maryland, 1996.

[8] W. Hwang, Y.-K. Kim, and M. E. Rudd, J. Chem. Phys. **104**, 2956 (1996).

[9] L. H. Toburen, Radiat. Environ. Biophys. **37**, 221 (1998).

[10] F. A. Cucinotta, R. Katz, and J. W. Wilson, Radiat. Environ. Biophys. **37**, 259 (1998).

[11] W. E. Wilson and H. Nikjoo, Radiat. Environ. Biophys. **38**, 97 (1999).

[12] C. A. Tobias, E. A. Blakely, F. Q. H. Ngo, and T. C. H. Yang, in *Radiation Biology and Cancer Research*, edited by R. A. Meyn and H. R. Withers (Ravan Press, New York, 1980), pp. 195–230.

[13] D. Ohsawa, H. Kawauchi, M. Hirabayashi, Y. Okada, T. Honma, A. Higashi, S. Amano, Y. Hashimoto, F. Soga, and Y. Sato, Nucl. Instrum. Methods Phys. Res. B **227**, 431 (2005).

[14] M. E. Rudd, Phys. Rev. A **38**, 6129 (1998).

[15] H. Böckl and F. Bell, Phys. Rev. A **28**, 3207 (1983).

[16] P. D. Fainstein, V. H. Ponce, and R. D. Rivarola, J. Phys. B **24**, 3091 (1991).

[17] E. Fermi, Phys. Rev. **75**, 1169 (1949).
[18] G. Lanzanó, E. De Filippo, D. Mahboub, H. Rothard, S. Aiello, A. Anzalone, S. Cavallaro, A. Elanique, E. Geraci, M. Geraci, F. Giustolisi, A. Pagano, and G. Politi, Phys. Rev. Lett. **83**, 4518 (1999).
[19] G. Lanzanó, E. De Filippo, S. Aiello, M. Geraci, A. Pagano, Sl. Cavallaro, F. Lo Piano, E. C. Pollacco, C. Volant, S. Vuillier, C. Beck, D. Mahboub, R. Nouicer, G. Politi, H. Rothard, and D. H. Jakubassa-Amundsen, Phys. Rev. A **58**, 3634 (1998).
[20] B. Sulik, Cs. Koncz, K. Tokési, A. Orbán, and D. Berényi, Phys. Rev. Lett. **88**, 073201 (2002).
[21] U. Bechthold, J. Ullrich, U. Ramm, G. Kraft, S. Hagmann, C. O. Reinhold, D. R. Shultz, and H. Schmidt-Böcking, Nucl. Instrum. Methods Phys. Res. B **146**, 46 (1998).
[22] C. O. Reinhold, D. R. Schultz, U. Bechthold, G. Kraft, S. Hagmann, and H. Schmidt-Böcking, Phys. Rev. A **58**, 2611 (1998).
[23] L. H. Toburen, Phys. Rev. A **9**, 2505 (1974).
[24] Yong-Ki Kim, Phys. Rev. A **6**, 666 (1972).
[25] M. Inokuti, Rev. Mod. Phys. **43**, 297 (1971).
[26] F. Bell, H. Bockl, M. Z. Wu, and H.-D. Betz, J. Phys. B **16**, 187 (1983).
[27] H. Hidmi, P. Richard, J. M. Saunders, H. Schöne, J. P. Giese, D. H. Lee, T. J. M. Zouros, and S. L. Varghese, Phys. Rev. A **48**, 4421 (1993).
[28] G. Lanzanó, E. De Filippo, D. Mahboub, H. Rothard, S. Aiello, A. Anzalone, S. Cavallaro, A. Elanique, E. Geraci, M. Geraci, F. Giustolisi, A. Pagano, and G. Politi, Phys. Rev. Lett. **83**, 4518 (1999).
[29] G. Lanzanó, E. De Filippo, S. Aiello, M. Geraci, A. Pagano, Sl. Cavallaro, F. Lo Piano, E. C. Pollacco, C. Volant, S. Vuillier, C. Beck, D. Mahboub, R. Nouicer, G. Politi, H. Rothard, and D. H. Jakubassa-Amundsen, Phys. Rev. A **58**, 3634 (1998).
[30] M. M. Jakas, Phys. Rev. A **52**, 866 (1995).
[31] D. Ohsawa, Y. Sato, Y. Okada, V. P. Shevelko, and F. Soga, Phys. Lett. A **342**, 168 (2005).
[32] D. H. Lee, P. Richard, T. J. M. Zouros, J. M. Sanders, J. L. Shinpaugh, and H. Hidmi, Phys. Rev. A **41**, 4816 (1990).
[33] J. C. Ashley, R. H. Ritchie, and W. Brandt, Phys. Rev. B **5**, 2393 (1972).
[34] H. Bichsel, Phys. Rev. A **41**, 3642 (1990).
[35] V. P. Shevelko, Th. Stöhlker, and I. Yu. Tolstikhina, Nucl. Instrum. Methods Phys. Res. B **184**, 295 (2001).
[36] S. Uehara and H. Nikjoo, J. Phys. Chem. B **106**, 11051 (2002).
[37] W. A. Mckinley and H. Feshback, Phys. Rev. **74**, 1759 (1948).